Systemic Delivery of Tumor-Targeted Bax-Derived Membrane-Active Peptides for the Treatment of Melanoma Tumors in a Humanized SCID Mouse Model

Anastassia Karageorgis, Michaël Claron, Romain Jugé, Caroline Aspord,
Fabien Thoreau, Claire Leloup, Jérôme Kucharczak, Joël Plumas, Maxime
Henry, Amandine Hurbin, et al.

HAL Id: hal-02000186
https://hal.archives-ouvertes.fr/hal-02000186

Submitted on 15 Jan 2020

Systemic Administration of Tumor-Targeted Bax-Derived Membrane-Active Peptides

for the Treatment of Human Melanoma Tumors in a Humanized SCID Mouse Model

Anastassia Karageorgis[1,2*,] Michaël Claron[2,3*], Romain Jugé[4*], Caroline Aspord[2,6,7]**, Fabien Thoreau[1,2,3]**, Claire Leloup[2,6,7], Jérôme Kurcharczak[4], Joël Plumas[2,6,7], Maxime Henry[1,2], Amandine Hurbin[1,2], Pascal Verdié[5], Jean Martinez[5], Gilles Subra[5], Pascal Dumy[3,5], Didier Boturyn[2,3], Abdel Aouacheria[4,8$], Jean-Luc Coll[1,2,$]

[1] INSERM U1209, Institut Albert Bonniot, Grenoble, F-38000, France
[2] Université Grenoble Alpes, Grenoble, F-38000, France
[3] CNRS UMR 5250, ICMG FR2607, Grenoble, F-38000, France
[4] Molecular Biology of the Cell Laboratory (LBMC), Ecole Normale Supérieure de Lyon, UMR 5239 CNRS – UCBL – ENS Lyon, 46 Allée d'Italie, 69364 Lyon Cedex 07, France
[5] CNRS UMR 5247, Institut des Biomolécules Max Mousseron IBMM, Montpellier, F-34095, France
[6] EMR EFS-UGA-INSERM U1209- CNRS, Immunobiology and Immunotherapy of Chronic Deseases, La Tronche, F-38706 France
[7] EFS Rhone-Alpes, R&D Laboratory, La Tronche, F-38701, France
[8] ISEM - Institut des Sciences de l'Evolution de Montpellier, UMR 5554, Université de Montpellier | CNRS | IRD | EPHE, Place Eugène Bataillon, 34095 Montpellier, France

* Co- first authors
** Co-2nd Authors

[$] Corresponding authors:

Jean-Luc Coll:
IAB; Institute for Advanced Biosciences
CRI UGA / Inserm U1209 / CNRS UMR 5309
Site santé – Allée des Alpes
38700 La Tronche
Electronic address: jean-luc.coll@univ-grenoble-alpes.fr

Abdel Aouacheria:
ISEM, Institut des Sciences de l'Evolution de Montpellier
UMR 5554, Université de Montpellier | CNRS | IRD | EPHE
Place Eugène Bataillon
34095 Montpellier, France

Electronic address: abdelouahab.aouacheria@umontpellier.fr.

ABSTRACT

Melanoma is a highly metastatic and deadly form of cancer. Invasive melanoma cells overexpress integrin $\alpha_v\beta_3$, which is a well-known target for Arg-Gly-Asp-based (RGD) peptides. We developed a sophisticated method to synthetize mg amounts of a targeted vector that allows the RGD-mediated targeting, internalization and release of a mitochondria-disruptive peptide derived from the pro-apoptotic Bax protein. We found that 2.5 µM of Bax [109-127] was sufficient to destabilize the mitochondria in 10 different tumor cell lines, even in the presence of the anti-apoptotic Bcl2 protein, which is often involved in tumor resistance. This pore-forming peptide displayed antitumor activity when it was covalently linked by a disulfide bridge to the tetrameric RAFT-c[RGD]$_4$-platform and after intravenous injection in a human melanoma tumor model established in humanized immuno-competent mice. In addition to its direct toxic effect, treatment with this combo induced the release of the immuno-stimulating factor MCP1 in the blood and a decrease in the level of the pro-angiogenic factor FGF2. Our novel multifunctional, apoptosis-inducing agent could be further customized and assayed for potential use in tumor-targeted therapy.

Introduction

Melanoma is a common and devastating form of skin cancer. It is highly metastatic and resistant to chemotherapy and radiotherapy. It is known to progress initially in a radial growth phase. In this phase, melanoma cells accumulate mutations. This process is followed by a vertical phase, in which the cells invade the dermis and produce angiogenic factors that induce new blood vessel formation. This 'angiogenic switch' has been associated with aggressiveness and is characterized by the modulation of the expression of several genes, including those encoding for $\alpha_v\beta_3$ integrin [1-8] and VEGF receptors. Antagonists of $\alpha_v\beta_3$ integrin, such as cyclic Arg-Gly-Asp (RGD)-containing peptides and c[RGDfV] [9, 10], have been under investigation as antiangiogenic agents for decades [11]. These investigations produced Cilengitide (EMD 121974) [12], which initially showed promising results for breast tumor therapy. [13] Phase II trials were then conducted for the treatment of prostate cancer [14, 15], followed by phase III trials for the treatment of glioblastoma; however, it was ultimately discontinued as an anticancer drug because it did not improve outcomes. [16] This failure was explained by the observation that low doses of Cilengitide actually stimulate VEGF-induced angiogenesis instead of producing the expected antiangiogenic activity [17] and that Cilengitide can enhance tumor growth by augmenting the activity of tumor-promoting M2 macrophages [18].

RGD-based peptides have been more successful as targeted imaging probes [19], as shown in melanoma patients [20]. At the preclinical level, it also served as a drug delivery system [21-25]. In previous work, we took advantage of the integrin-clustering capacity of a tetravalent cRGD-containing peptide [26] to generate more effective antagonists with augmented specificity for tumors [27-30], improved cellular uptake [31, 32] and enhanced toxicity upon association with pro-

apoptotic peptides. [33, 34] The tumor-targeted delivery of cytotoxic peptides (e.g., (KLAKLAK)$_2$) was initially of interest for the treatment of tumors [35-38], particularly melanoma, when targeted by cRGD [39] or with a Cell-Penetrating Peptide, such as TAT [40]. However, despite promising results, no follow-up studies have been reported on these compounds, certainly because of the modest activity of (KLAKLAK)$_2$ [41].

The aim of this study was to develop an original pathway to generate second-generation RGD-targeted toxic peptides derived from the putative pore-forming domain of Bax (a pro-apoptotic protein belonging to the Bcl-2 family) that would directly induce the release of mitochondrial cytochrome c. We previously demonstrated that a synthetic peptide derived from the 5th helix of Bax exhibits high mitochondrial membrane-destabilizing activity [42] and induces the caspase-dependent apoptosis of cancer cells when fused to a polyarginine cell-penetrating peptide [43]. Our data indicated that mitochondrial perforation, which ultimately leads to cell suicide, is very rapid and occurs independently of endogenous executors of the Bcl-2 family, such as Bax and Bak. Preliminary *in vivo* studies using mouse xenograft models further demonstrated that this molecule, named "poropeptide," has potent anticancer activity after intratumoral administration. Here, we describe the truncation, optimization and characterization of this active peptide grafted to the RGD-presenting platform, yielding a conjugate termed Poro-Combo, through a set of *in vitro* and *in vivo* experiments in humanized mice bearing human melanoma tumors.

Material and Methods

Cell Culture

Three different adherent malignant human melanoma cell lines were used in the study: A375, Colo829 and Me275. Colo829 and A375 cells lines were purchased from ATCC (American Type Culture Collection, Molsheim, France**)** and cultured at 37°C and 5% CO2 in DMEM and RPMI-1640, respectively, (PAA) supplemented with 10% FBS, 1% penicillin-streptomycin and 2 mM L-glutamine (Sigma-Aldrich). Me275 cells are not commercialized and were kindly provided by Pr J-C Cerottini (Ludwig Institute for Cancer Research, Epalinges, Switzerland). Me275 cells were cultured at 37°C and 5% CO2 in RPMI-1640 (PAA) supplemented with 10% FBS, 1% penicillin-streptomycin and 2 mM L-glutamine (Sigma-Aldrich). Stable transfectants of NIH 3T3 cells expressing GFP or GFP-Bcl-2 were kindly provided by Dr. Nathalie Bonnefoy (INSERM U851). MeWo and SK-MEL-28 cells were obtained from the CelluloNet Biobank (BB-0033-00072, Centre de Ressources Biologiques of UMS3444/US8).

Peptides

The sequences of the peptides are shown in Supp Table 1. Colicin, delta-endotoxin and diphtheria toxin peptide derivatives were purchased from GeneCust EUROPE (Dudelange, Luxembourg) at a 2 or 5 mg scale with purity > 95%. Other peptides were synthesized by the SynBio3 IBISA platform, Montpellier or the ICMG Chemistry Nanobio, Grenoble facilities. The assembly of all linear protected peptides was performed either manually or automatically by solid-phase peptide synthesis (SPPS) using the standard 9-fluorenylmethoxycarbonyl/tertiobutyl (Fmoc/tBu) protection strategy. Cyclization reactions

were carried out as described [26]. RAFT-c[RGD]$_4$ was obtained using oxime ligation in solution as previously described [33].

RAFT-c[RGD]$_4$-S-S-depsi-cgg-Poro2D was obtained from the depsi cgg-Poro2D peptide (6.8 mg, 2.43 µmol) and nitro-pyridine sulfenyl-containing RAFT-c[RGD]$_4$ (10 mg, 2.42 µmol) dissolved in 500 µL of ACN/PBS (pH 4.8, 1/3) under argon. The reaction mixture was stirred for 5 min at room temperature under argon. The product was purified by RP-HPLC and obtained as a white powder (8.4 mg, 1.33 µmol, 55%). RAFT-c[RAD]$_4$ was used as negative control that did not bind the integrin. Indeed, c[-RßADfK-] was a nonsense peptide in which the Gly residue of Arg-Gly-Asp (RGD) had been changed to ßAla.

Mitochondrial assays

Crude, intact mitochondria were prepared as previously described [42]. In brief, cells were mechanically broken using a 2 mL glass/glass dounce homogenizer (Kontes) (30 strokes). The homogenates were cleared at 1500 g, and the mitochondria were spun down at 10 000 g. Cholesterol depletion in the mitochondrial membranes was achieved by treatment with Me-β-cyclodextrin (β-MCD, Sigma-Aldrich) as previously described [44]. Cholesterol enrichment was achieved by incubating isolated mitochondria with a cholesterol-BSA complex as described in [45]. For cytochrome c release assays, 30 mg of crude mitochondria was resuspended at 1 mg/mL in KCl buffer supplemented with succinate (5 mM) and EGTA (0.5 mM). Peptides were added to the samples at various concentrations, and incubations were carried out at 30°C under agitation (300 rpm). At the indicated time points, the samples were centrifuged (5 min, 10 000 g, 4°C) The supernatants and pellets were recovered and analyzed by immunoblotting for cytochrome c. Western blot analysis was performed according to standard procedures using monoclonal anti-cytochrome c antibody (BD Pharmingen) or Anti mPDK1 (Abcam) or

Anti mHSP70 (Abcam) as primary antibody and HRP-conjugated goat anti-mouse (Dako) as secondary antibody.

Cellular viability evaluation

The cellular viability of Me275 and Colo829 tumor cells was evaluated using a colorimetric MTT test measuring mitochondrial activity. A375 and Colo829 cells were plated in 96-well plates at 1.5×10^4 cells/well. 24 h later, the cells were treated with RAFT-c(RGD)4-poro2 at 1, 2.5, 5 or 10 µM, while control group received the vehicle alone. A positive control of apoptosis was done by treating cells with 1 µM staurosporine. One day after treatment, the cell culture medium was replaced by 100 µL of uncolored DMEM-containing 10% MTT (Calbiochem®). The cells were incubated for 4 h at 37°C. The MTT crystals were solubilized with 100 µL of a solution containing 12.5 mL Triton 100%, 1.25 mL HCl 10N and 125 mL anhydrous isopropanol. The optical density was evaluated using a Beckamn Coulter AD340 spectrophotometer at 570 nm and 620 nm.

Apoptosis assays

Me275, Colo829 and A375 cells were seeded in 12-well plates. The cells were treated for 24 hours with RAFT-c(RGD)4-poro2 at concentrations ranging between 0.5 and 10 µM. Control cells were treated with RAFT-c(RGD)4 or the vehicle alone. Active Caspase 3 was evaluated by flow cytometry using Active Caspase 3 Apoptosis Kit (Becton Dickinson, Pont de Claix, France) on an Accuri-C6 flow cytometer with a filter (585/42 nm) and the CflowPlus software.

Biodistribution and tumor targeting in vivo

One million A375 or Colo829 human melanoma cells were implanted on the right flank of humanized mice. Then, 200 µL of RAFT-c(RGD)$_4$-A700 50 µM (Fluoptics, France) was intravenously injected into the mice. 2D-Fluorescence reflectance imaging was performed as previously described 24 h after the injection on isolated organs using a Hamamatsu photonics device [27]. Fluorescence was visualized at 660 nm (i) and quantified (ii) in different organs using the Wasabi® software.

In vivo anti-tumor activity of Poro-Combo in Humanized mice

NOD-SCID IL2RγC-/- immunodeficient mice (NOD.Cg-Prkdcscid Il2rgtm1Wjl/SzJ) were purchased from Jackson ImmunoResearch Laboratories (Bar Harbor, USA) and bred at the Plateforme de Haute Technologie Animale (PHTA, La Tronche, France). Humanized mice were constructed by transplanting intravenously 1-2.10^5 HLA-A0201$^+$ CD34$^+$ hematopoietic progenitor cells purified from umbilical cord blood into sub-lethally irradiated 4-week-old NOD-SCID IL2RγC$^{-/-}$ mice (100-110 cGy). The CD34$^+$ hematopoietic progenitor cells (HPC) were positively isolated from the mononuclear fraction using anti-CD34 magnetic microbeads and MS separation columns (Miltenyi Biotec). The purity was routinely approximately 90%. Twelve weeks after reconstitution, 10^6 human melanoma tumor cells (Me275 cell line) were subcutaneously implanted into the flank of humanized mice. The animals were then treated with daily intraperitoneal injections of 200 µl of either saline (PBS) or a solution containing 0.132 µmol of the following molecules: Poro 2, RAFT-c(RGD)$_4$, RAFT-c(RAD)$_4$-poro 2, or RAFT-c(RGD)$_4$-poro 2. Note that we did not evaluate the absence of targeting with the RAFT-c(RAD)$_4$ peptide because we have already tested this in many different tumor models [27, 29, 34], including melanoma [46]. Tumor size was monitored every day, and tumor volume was calculated using the formula: (short diameter)^2 x long diameter/2. The procedures for human

cells were approved by the French Blood Service's Institutional Review Board. Animal studies were carried out in accordance with European regulations and the French National Charter guidelines. The protocol was approved by the Ethics Committee from Grenoble (approval # 211-UHTA-U823-CA-08) and registered at the National Ministry under the number #01993.

Immunohistology

At the end of the treatment, tumors were taken and frozen in Tissue-Tek[®] (Sakura Finetek, Villeneuve d'Ascq) and stored at -80°C. Immunohistology was then performed on 7 μm tumor slices. Tumor cell proliferation was evaluated using a rabbit anti-mouse Ki67 antibody (DakoCytomation) associated with the rabbit anti-rat HRP secondary antibody (DakoCytomation) on tumor slices fixed in acetone. Apoptosis was evaluated using a rabbit primary antibody against cleaved caspase 3 (Asp 175) (Cell signaling) associated with the secondary antibody anti-rabbit IgG HRP (Trueblot). Blood vessels were observed by immunohistology on tumor slices fixed with acetone using a rabbit primary anti-CD31 antibody (Abcam[®]) associated with the secondary antibody anti-rabbit IgG HRP (Trueblot). All staining was observed using an Olympus BX41 microscope and the AnalySIS software with a color DP70 camera.

Dosage of angiogenic factors and chemokines in the plasma

Blood was collected before and at different time points after the start of the treatment. Human angiogenin, FGF-2, MCP1 and IP10 were quantified in the plasma by a Cytometric Bead Array (CBA, BD) using a FACSCanto II and the FCAP Array software (BD).

Evaluation of anti-tumor immunity

At the end of the treatment, the infiltration and functional status of immune cells were evaluated at the tumor site, in the draining lymph nodes (DLN), in the control lymph nodes (CLN) and in the spleen by flow cytometry. The organs were digested 30 min at 37°C with 2 mg/ml collagenase D (Roche Diagnostics). The resultant cell suspensions were washed with PBS with 2% FCS, stained using anti-human antibodies and submitted to flow cytometry analysis on a FACSCalibur using the CellQuest Pro software (BD). The anti-human CD45, CD3, CD8, CD56 (Beckman), CD69, and CD107 (BD) antibodies were used, as was HLA-A*0201/MelA dextramers (Immudex).

Statistical analysis

Student's t-tests were run to compare the different groups using the GraphPad Prism 6® software.

Results

1/ Poropeptide selection

We previously developed a first-generation active peptide derived from the sequence of Bax ($_{106}$NWGRVVALFYFASKLVLKALSTKVPELIR$_{134}$, herein termed Bax [106-134]) [43], a protein evolutionarily functionalized to form pores in the mitochondrial outer membrane. This natural peptide is able to specifically target and permeabilize mitochondrial membranes, unlike analogous segments derived from structurally similar pore-forming toxins (Supp Figure 1). This peptide can also induce cell death at 10 µM [43], but only if it is covalently linked to a Cell-Penetrating Peptide, such as R8. Because this pore-forming peptide was 29 amino acids (aa) long, our first objective was to define its smallest toxic domain (Figure 1A). A series of eleven shorter C-terminally amidated analogues of Bax [106-134] were synthesized (Sup Table 1). The sequences were truncated both at the C- and N- terminus and assayed for their capacity to induce cytochrome-c release from purified mitochondria *in vitro* in comparison with the original Bax [106-134] peptide. As shown in Figure 1A, Bax [109-127] was efficient at 2.5 µM instead of 10 µM. All attempts to further reduce its length while keeping substantial pore-forming activity against mitochondria were unsuccessful. Indeed, the removal of the residues at the N-terminus proved to be deleterious to its activity (cf. Bax [112-127]), as was the removal of residues at the C-terminus (cf. Bax [109-124], Bax [109-125] and Bax [109-126]). We thus selected the peptide Bax [109-127], H-RVVALFYFASKLVLKALST-NH$_2$, called Poro2, and verified that it was sufficient to permeabilize the mitochondria extracted from 10 different tumor cell lines (Figure 1B). Because cholesterol [47] and Bcl2 can potentially reduce the toxicity of this pore-forming peptide, we also demonstrated that Poro2 activity was insensitive to the concentration of cholesterol or to the presence of Bcl2 in purified mitochondria (Sup Figure 2). This result is important because it shows that Poro2 will be toxic on a large panel of target cells (including

cancer cells) with variable cholesterol and Bcl2 contents, consistent with the positive data obtained using multiple cell lines (Figure 1B).

The next step was the derivatization of a Poro2 lead sequence for conjugation *via* a disulfide bridge and a spacer to the targeting scaffold RAFT-c[RGD]$_4$. We introduced a sulfhydryl group at the N-terminus of Poro2 by adding a Cysteine-Glycine-Glycine sequence. We used D-amino acids to reduce protease degradation, forming the so-called cgg-Poro2D pore-forming peptide that was still active on purified mitochondria (Figure 1C), while sparing the plasma membranes of cultured human cells (Supp Figure 3).

2/ Scaled-up production of the peptides

Before grafting our second-generation poropeptide to the targeting moiety RAFT-c[RGD]$_4$, we sought to optimize the synthesis strategy of cgg-Poro2D. Indeed, the handling and purification of cgg-Poro2D was troublesome because of its poor solubility. This difficulty, although it is classical in the field of pharmaceuticals, represents a serious limitation for its use, even during the conjugation step. We hypothesized that the amphipathic helical structure of poro-derivatives contributes to their poor solubility. To overcome this limitation, we utilized the residue Serine118, which is located in the center of the active sequence, to design a depsipeptic derivative of cgg-Poro2 (Figure 2). The displacement of the peptidic chain from the α amino group to the hydroxyl of a serine side chain was proposed simultaneously by the groups of Kiso [48] and Mutter [49] to handle the synthesis of aggregating sequences. The O-acylated derivative of the peptide may undergo an O-N acyl shift in neutral or basic conditions to yield the desired linear peptide sequence. The depsipeptidic derivative offers a double advantage for solubility enhancement. First, after cleavage from the resin and the removal of the N-protecting group of serine in acidic conditions, the depsipeptide 'gains' a

protonatable functional group, such as the Nα-amino group of the serine residue, which enhances its solubility. Second, the depsipeptide is a β-branched peptide in which the amide bond is replaced by an ester. These modifications impact the establishment of intra- and inter-molecular hydrogen bonding, thereby affecting the formation of secondary structures and aggregation. Before performing the synthesis with expensive D-amino acids, the strategy was first evaluated for Poro2 (Sup Figure 4), and the optimized strategy was then applied to depsi cgg-Poro2D. After purification and freeze drying, the overall yield was 7%. More than two hundred mg of the depsi cgg-Poro2D form of Bax[109-127] were obtained for conjugation with the Npys cysteine derivative of RAFT-c[RGD]$_4$.

A modular synthesis strategy was then adopted to construct the bifunctional molecules (Figure 3). We chose chemoselective ligations, such as stable oxime bonds, to connect the aldehyde-bearing 'homing' RGD motif and a cleavable disulfide linker serving to attach the pro-apoptotic depsi-cgg-Poro2D peptide. The synthesis of a cyclodecapeptidic intermediate bearing protected an aminooxy functional group was then carried out using Nε-modified lysine in which the aminooxy moiety is protected by a 1-ethoxyethylidene group (Eei). This protective group was shown to be fully compatible with standard SPPS conditions [50]. The Alloc protective group at a lysine side chain was necessary to append a cysteine encompassing the activating nitro-pyridine sulfenyl residue. To append the targeting elements to the cyclodecapeptidic scaffold, we performed an aminooxy deprotection and an oxime ligation of the appropriate cyclopentapeptidic cyclo[-RGDfK(-COCHO)-] in one-pot reactions. The subsequent ligation of depsi-cgg-Poro2D was carried out under mild acidic conditions (pH 4.8) under argon for 5 min. The reactions were carefully monitored by HPLC (Figure 4). After 5 minutes, the disulfide bond formation in the soluble depsi cgg-Poro2D peptide (Figure 4 (b)) and the RAFT c[RGD]$_4$ (Figure 4 (a)) was complete, providing the expected final

compound (Figure 4 (c)). The products were directly recovered after RP-HPLC purification in satisfying yields (~ 55%).

3/ In vitro evaluation of RAFT-c[RGD]4-S-S- depsi-cgg-Poro2D

The toxicity of RAFT-c[RGD]$_4$-S-S-depsi-cgg-Poro2D containing Bax[109-127]$_D$ (subsequently called Poro-Combo) was then tested on melanoma tumor cell lines (Figure 5). The cell viability was evaluated using an MTT assay one day after incubation with Poro-Combo, as shown in Figure 5A. Dose-dependent toxicity was visible, and only 40% of melanoma cells were still alive in the presence of 10 µM Poro-Combo. This cytotoxic effect is identical to that observed with 1 µM of the positive control Staurosporine.

Cell death was associated with the activation of caspase 3 (Figure 5B), indicating that the toxic peptides were inducing caspase-dependent apoptosis. This cell-death-inducing activity was not detectable when the cells were incubated with the control RAFT-RGD peptides devoid of the Poro2 moiety.

4/ In vivo evaluation

Human melanoma xenografts are exciting experimental models that mimic the biological behavior of malignant melanoma, which is a highly dangerous form of skin cancer. Before investigating the antitumor activity of Poro-Combo *in vivo*, we verified that the fluorescent RAFT-c[RGD]$_4$-Alexa Fluor700 compound was able to target human Me275 melanoma xenografts implanted in mice (Sup Figure 5). Subcutaneous tumors were found to be strongly fluorescent 5 h and 24 h after the intravenous injection of the targeting agent, and the fluorescence intensity of the tumor site was only slightly lower than that of the kidneys. Using

confocal fluorescence imaging of the cryosections of these tumors, we detected the presence of intracellular RAFT-c(RGD)$_4$-A700 in the tumor cells located in the immediate vicinity of afferent blood vessels (Sup. Fig. 5C).

To evaluate the direct anti-tumor activity of Poro-Combo *in vivo* and the possible appearance of an anti-tumor immune response because of the induction of an immunogenic tumor cell death, we developed a human tumor model in NOD-SCID IL2RγC-/- mice reconstituted with a human immune system. This was performed by first engrafting human CD34+ hematopoietic progenitor cells (HPCs) and then human tumor cells. Three months after the graft of human CD34 HPCs, the humanized mice received a subcutaneous injection of Me275 melanoma cells on their flank. One week later, these animals were treated with repeated daily IP injections of 200 µL of a solution containing 0.132 µmol of the different polypeptides (Sup Figure 6). Poro-Combo treatment resulted in a statistically significant prevention of tumor growth (p=0.0095) (Figure 6 A and B), in contrast to all other treatments.

Immunohistology performed on the different tumors demonstrated that a significant reduction of tumor cell proliferation was induced by the Poro-Combo treatment (Figure 7), as shown after Ki67 immunostaining. This effect did not reflect a statistically significant induction of tumor cell apoptosis. In contrast, no detectable differences were found between the number of CD31-positive blood vessels counted in the different tumors.

No acute toxicity was observed in all treated animals. Liver and kidney biopsies also showed unaffected tissues, which confirms the absence of non-specific cell killing activity in these major organs (Sup Fig. 8).

We finally examined whether Poro-Combo-mediated cell death induced an antitumor immune reaction. We detected an infiltration of human CD45+ immune cells in the treated tumors that was composed of potential anti-tumor effectors, such as T cells and NK cells. However, no

differences in the term of proportion of infiltrating cells, activation level (CD69) and function (CD107 level) of these cells could be found among the groups, nor for tumor-specific CD8 T cells assessed using dextramer staining (Sup Figure 7).

The dosages of the plasmatic levels of Angiogenin, FGF-2, MCP1 and IP10 were assessed during the mice treatments. As shown in Figure 8, an interesting augmentation of the chemo-attractant molecule MCP1 was detected specifically in the plasma of Poro-Combo-treated mice, suggesting that immune infiltration and activation were promoted at the tumor site. Interestingly, Poro-Combo treatment was associated with a clear diminution of the plasmatic levels of the pro-angiogenic factor FGF-2, which became undetectable as soon as 2 days after the start of the treatment (d9). This effect could be related to Poro-Combo toxicity of tumor cells and tumor-activated stromal cells and possible anti-angiogenic potential.

Discussion

In the present study, we generated a chemically sophisticated tumor-targeted therapeutic peptide that contains a multivalent RGD-targeting head and a toxic "poro2" small fragment derived from the Bax pro-apoptotic protein. To overcome solubility issues, a special method was applied that yielded the successful synthesis of a depsipeptic derivative of the "poro2" moiety. This engineered compound offers the benefit of enhanced solubility and the ability to switch and return to a classical peptidic sequence under physiological pH. This toxic peptide is covalently anchored to the targeting head *via* a cleavable disulfide bridge, thus allowing it to be released into the cytoplasm.

Since the pioneering work of Ellerby *et al.* in 1999 [35], many efforts have been made to generate tumor-targeted toxic peptides initially based on the 14-amino-acid antimicrobial peptide KLAKLAKKLAKLAK, called (KLAKLAK)$_2$. Since then, different death-inducing peptides were targeted for tumor cells *via* various specific ligands, such as CNGRC, RGD, anti Neuropilin-1 (NRP-1) or E-selectin binding peptides, as well as with small ligands, such as folic acid [51-54]. The amphipathic toxic peptides are characterized by their positive charges, which enable them to bind to negatively-charged cell membranes and cause their disruption, eventually leading to cell death. Their mode of action can vary. It was shown that they can induce necrosis after plasma membrane disruption, depending on their L- or D- chirality [55, 56], apoptosis by the up-regulation of caspases [57], the influx of extracellular Ca_2^+, Ca_2^+-mediated $\Delta\Psi$m disruption and mitochondrial $O_2^{\cdot-}$ generation [58]. However, the cationic peptide (KLAKLAK)$_2$ has been reported to have a potency that is too low for it to be used as an effective anticancer drug [41].

As BH3-only proteins either directly or indirectly inhibit prosurvival BCL-2 family members, such as BCL-2, BCL-xL and MCL-1, to increase cellular sensitivity to anticancer agents,

efforts were made to develop so-called BH3 mimetics [59]. Some have entered clinical trials (reviewed in [60]). A short peptide derived from the orphan nuclear receptor Nur77 was shown to bind the N-terminal regulatory region of the anti-apoptotic protein Bcl-2 and convert it into a pro-apoptotic killer protein [61]. More recently, a pro-necrotic peptide derived from Noxa, a BH3-only protein of the Bcl-2 family, was described for its capacity to induce necrosis in tumor cells in a caspase-independent manner when associated with a NRP-1-targeting peptide [51].

However, one major limitation common to both the BH3-mimetic approach and the targeting of non-BH3 sites is their strict dependency on the endogenous levels of the anti-apoptotic Bcl-2 family of proteins expressed in tumor cells. Moreover, such molecules are also expected to be less effective in tumor cells that are mutated or deficient in pro-apoptotic Bax or Bak, which are two critical complementary effectors of apoptosis. The pro-apoptotic Bax protein contains structurally defined membrane-interacting regions [62], some of them (α1, α9, α5, α6 and a central α5α6-hairpin motif) with presumed membrane-targeting functions [63-65]. It has been previously shown that peptides corresponding to the first and/or second helix of the central domain of Bax can reproduce the poration activity displayed by the full-length parent protein. Hence, the central helices (α5-α6) of Bax carry the minimal structural information to form pores in lipid membranes, similar to amphipathic peptide antibiotics [66-70]. We previously established that a 29-residue peptide (Poro1) corresponding to the extended 5th helix of Bax can disrupt the mitochondrial membrane, inducing $\Delta\Psi$m loss and cytochrome c release [43]. This Bax-derived peptide was more efficient than (KLAKLAK)$_2$ or the BH3 peptidic domain of Bax in inducing apoptosis in tumor cells in vitro. Finally, when it was fused to a polyarginine transduction motif, it had potent anticancer activity in nude mice bearing human cancer xenografts.

In the present work, we reduced the length of this first-generation Bax-derived poropeptide to its minimal toxic domain and showed that this so-called Poro2 peptide was efficient in inducing cytochrome-c release from mitochondria from a large panel of tumor cell lines (n=10). Furthermore, its mitochondria-disruptive activity was insensitive to the presence of cholesterol or antiapoptotic Bcl2. This was still true when the active peptide was synthesized as a D-enantiomer form, and we proved that it did not affect the integrity of the plasma membrane, instead acting preferentially on the mitochondrial compartment. Based on these promising results, we decided to link this second-generation poropeptide *via* a labile bond to a multimeric RGD-based tumor targeting agent. We chose RAFT-c[RGD]$_4$, as our previous results established that this cargo is an excellent tumor targeting vector, but more importantly, because it allows the active clustering and internalization of the $\alpha_v\beta_3$ integrin receptor [31], followed by an efficient intra-cytoplasmic release after reduction of the S-S bridge [71]. Our data demonstrate that in its final conjugated form (Poro-Combo), our functionalized cargo actively targeted melanoma tumors *in vivo* after intravenous injection and induced tumor growth inhibition. We paid particular attention to the tumor model that we chose because we wanted to evaluate whether the therapeutic activity generated *in vivo* also involved antitumor-immune activity that would be primed by Poro-Combo [72, 73]. Indeed, melanoma is a form of cancer characterized by its high immunogenicity, which is also known to generate an immunosuppressive microenvironment [74]. Thus, it was important to evaluate whether the death of tumor cells triggered by Poro-Combo could provoke an immunogenic response. To this end, we generated humanized mice carrying human melanoma tumors. In this model, apoptosis induction was not very strong, and the most obvious phenotype under treatment was a reduction of tumor cell proliferation. In particular, we did not observe a significant increase in the number of infiltrating cells or their immune activation, which could have indicated the presence of activated T lymphocytes or tumor-cytolytic NK cells. However, in addition to the

direct toxicity of Poro-Combo for $\alpha_v\beta_3$ integrin-positive cells, the observed antitumor activity was associated with a clear diminution of the systemic level of FGF-2 associated with a concomitant increase in the chemoattractant molecule MCP1 in treated animals. This effect is of particular interest and needs to be further investigated.

In conclusion, herein, we described the design, synthesis and evaluation of a novel multifunctional, apoptosis-inducing agent that could be further customized, assayed and potentially used for tumor-targeted therapy.

REFERENCES

1. Meves, A, Nikolova, E, Heim, JB, Squirewell, EJ, Cappel, MA, Pittelkow, MR*, et al.* (2015). Tumor Cell Adhesion As a Risk Factor for Sentinel Lymph Node Metastasis in Primary Cutaneous Melanoma. *J Clin Oncol* **33**: 2509-2515.

2. Desgrosellier, JS, and Cheresh, DA (2010). Integrins in cancer: biological implications and therapeutic opportunities. *Nature reviews Cancer* **10**: 9-22.

3. Petitclerc, E, Stromblad, S, von Schalscha, TL, Mitjans, F, Piulats, J, Montgomery, AM*, et al.* (1999). Integrin alpha(v)beta3 promotes M21 melanoma growth in human skin by regulating tumor cell survival. *Cancer Res* **59**: 2724-2730.

4. Hsu, MY, Shih, DT, Meier, FE, Van Belle, P, Hsu, JY, Elder, DE*, et al.* (1998). Adenoviral gene transfer of beta3 integrin subunit induces conversion from radial to vertical growth phase in primary human melanoma. *Am J Pathol* **153**: 1435-1442.

5. Natali, PG, Hamby, CV, Felding-Habermann, B, Liang, B, Nicotra, MR, Di Filippo, F*, et al.* (1997). Clinical significance of alpha(v)beta3 integrin and intercellular adhesion molecule-1 expression in cutaneous malignant melanoma lesions. *Cancer Res* **57**: 1554-1560.

6. Brooks, PC, Clark, RA, and Cheresh, DA (1994). Requirement of vascular integrin alpha v beta 3 for angiogenesis. *Science* **264**: 569-571.

7. Gehlsen, KR, Davis, GE, and Sriramarao, P (1992). Integrin expression in human melanoma cells with differing invasive and metastatic properties. *Clin Exp Metastasis* **10**: 111-120.

8. Seftor, RE, Seftor, EA, Gehlsen, KR, Stetler-Stevenson, WG, Brown, PD, Ruoslahti, E*, et al.* (1992). Role of the alpha v beta 3 integrin in human melanoma cell invasion. *Proc Natl Acad Sci U S A* **89**: 1557-1561.

9. Gurrath, M, Muller, G, Kessler, H, Aumailley, M, and Timpl, R (1992). Conformation/activity studies of rationally designed potent anti-adhesive RGD peptides. *Eur J Biochem* **210**: 911-921.

10. Pfaff, M, Tangemann, K, Muller, B, Gurrath, M, Muller, G, Kessler, H*, et al.* (1994). Selective recognition of cyclic RGD peptides of NMR defined conformation by alpha IIb beta 3, alpha V beta 3, and alpha 5 beta 1 integrins. *The Journal of biological chemistry* **269**: 20233-20238.

11.   Allman, R, Cowburn, P, and Mason, M (2000). In vitro and in vivo effects of a cyclic peptide with affinity for the alpha(nu)beta3 integrin in human melanoma cells. *European journal of cancer* **36**: 410-422.

12.   Mas-Moruno, C, Rechenmacher, F, and Kessler, H (2010). Cilengitide: the first anti-angiogenic small molecule drug candidate design, synthesis and clinical evaluation. *Anticancer Agents Med Chem* **10**: 753-768.

13.   Burke, PA, DeNardo, SJ, Miers, LA, Lamborn, KR, Matzku, S, and DeNardo, GL (2002). Cilengitide targeting of alpha(v)beta(3) integrin receptor synergizes with radioimmunotherapy to increase efficacy and apoptosis in breast cancer xenografts. *Cancer Res* **62**: 4263-4272.

14.   Bradley, DA, Daignault, S, Ryan, CJ, Dipaola, RS, Smith, DC, Small, E, *et al.* (2010). Cilengitide (EMD 121974, NSC 707544) in asymptomatic metastatic castration resistant prostate cancer patients: a randomized phase II trial by the prostate cancer clinical trials consortium. *Invest New Drugs*.

15.   Alva, A, Slovin, S, Daignault, S, Carducci, M, Dipaola, R, Pienta, K, *et al.* (2012). Phase II study of cilengitide (EMD 121974, NSC 707544) in patients with non-metastatic castration resistant prostate cancer, NCI-6735. A study by the DOD/PCF prostate cancer clinical trials consortium. *Invest New Drugs* **30**: 749-757.

16.   Stupp, R, Hegi, ME, Gorlia, T, Erridge, SC, Perry, J, Hong, YK, *et al.* (2014). Cilengitide combined with standard treatment for patients with newly diagnosed glioblastoma with methylated MGMT promoter (CENTRIC EORTC 26071-22072 study): a multicentre, randomised, open-label, phase 3 trial. *Lancet Oncol* **15**: 1100-1108.

17.   Reynolds, AR, Hart, IR, Watson, AR, Welti, JC, Silva, RG, Robinson, SD, *et al.* (2009). Stimulation of tumor growth and angiogenesis by low concentrations of RGD-mimetic integrin inhibitors. *Nature medicine* **15**: 392-400.

18.   Su, X, Esser, AK, Amend, SR, Xiang, J, Xu, Y, Ross, MH, *et al.* (2016). Antagonizing Integrin beta3 Increases Immunosuppression in Cancer. *Cancer Res* **76**: 3484-3495.

19.   Chen, H, Niu, G, Wu, H, and Chen, X (2016). Clinical Application of Radiolabeled RGD Peptides for PET Imaging of Integrin alphavbeta3. *Theranostics* **6**: 78-92.

20.   Mena, E, Owenius, R, Turkbey, B, Sherry, R, Bratslavsky, G, Macholl, S, *et al.* (2014). [(1)(8)F]fluciclatide in the in vivo evaluation of human melanoma and renal tumors expressing alphavbeta 3 and alpha vbeta 5 integrins. *Eur J Nucl Med Mol Imaging* **41**: 1879-1888.

21. Hou, J, Diao, Y, Li, W, Yang, Z, Zhang, L, Chen, Z*, et al.* (2016). RGD peptide conjugation results in enhanced antitumor activity of PD0325901 against glioblastoma by both tumor-targeting delivery and combination therapy. *Int J Pharm* **505**: 329-340.

22. Gilad, Y, Noy, E, Senderowitz, H, Albeck, A, Firer, MA, and Gellerman, G (2016). Synthesis, biological studies and molecular dynamics of new anticancer RGD-based peptide conjugates for targeted drug delivery. *Bioorg Med Chem* **24**: 294-303.

23. Fu, X, Yang, Y, Li, X, Lai, H, Huang, Y, He, L*, et al.* (2016). RGD peptide-conjugated selenium nanoparticles: antiangiogenesis by suppressing VEGF-VEGFR2-ERK/AKT pathway. *Nanomedicine*.

24. Massaguer, A, Gonzalez-Canto, A, Escribano, E, Barrabes, S, Artigas, G, Moreno, V*, et al.* (2015). Integrin-targeted delivery into cancer cells of a Pt(IV) pro-drug through conjugation to RGD-containing peptides. *Dalton Trans* **44**: 202-212.

25. Cao, Q, Li, ZB, Chen, K, Wu, Z, He, L, Neamati, N*, et al.* (2008). Evaluation of biodistribution and anti-tumor effect of a dimeric RGD peptide-paclitaxel conjugate in mice with breast cancer. *Eur J Nucl Med Mol Imaging* **35**: 1489-1498.

26. Boturyn, D, Coll, JL, Garanger, E, Favrot, MC, and Dumy, P (2004). Template assembled cyclopeptides as multimeric system for integrin targeting and endocytosis. *J Am Chem Soc* **126**: 5730-5739.

27. Garanger, E, Boturyn, D, Jin, Z, Dumy, P, Favrot, MC, and Coll, JL (2005). New multifunctional molecular conjugate vector for targeting, imaging, and therapy of tumors. *Mol Ther* **12**: 1168-1175.

28. Garanger, E, Boturyn, D, Coll, JL, Favrot, MC, and Dumy, P (2006). Multivalent RGD synthetic peptides as potent alphaVbeta3 integrin ligands. *Org Biomol Chem* **4**: 1958-1965.

29. Jin, ZH, Josserand, V, Razkin, J, Garanger, E, Boturyn, D, Favrot, MC*, et al.* (2006). Noninvasive optical imaging of ovarian metastases using Cy5-labeled RAFT-c(-RGDfK-)4. *Mol Imaging* **5**: 188-197.

30. Jin, ZH, Josserand, V, Foillard, S, Boturyn, D, Dumy, P, Favrot, MC*, et al.* (2007). In vivo optical imaging of integrin alphaV-beta3 in mice using multivalent or monovalent cRGD targeting vectors. *Mol Cancer* **6**: 41.

31. Sancey, L, Garanger, E, Foillard, S, schoen, G, Hurbin, A, Albiges-Rizo, C*, et al.* (2009). Clustering and Internalization of Integrin alphavbeta3 With a Tetrameric RGD-synthetic Peptide. *Mol Ther* **17**: 837-843.

32. Jin, ZH, Razkin, J, Josserand, V, Boturyn, D, Grichine, A, Texier, I, *et al.* (2007). In vivo noninvasive optical imaging of receptor-mediated RGD internalization using self-quenched Cy5-labeled RAFT-c(-RGDfK-)(4). *Mol Imaging* **6**: 43-55.

33. Foillard, S, Jin, ZH, Garanger, E, Boturyn, D, Favrot, MC, Coll, JL, *et al.* (2008). Synthesis and biological characterisation of targeted pro-apoptotic peptide. *Chembiochem* **9**: 2326-2332.

34. Dufort, S, Sancey, L, Hurbin, A, Foillard, S, Boturyn, D, Dumy, P, *et al.* (2011). Targeted delivery of a proapoptotic peptide to tumors in vivo. *Journal of Drug Targeting* **19**: 582-588.

35. Ellerby, HM, Arap, W, Ellerby, LM, Kain, R, Andrusiak, R, Rio, GD, *et al.* (1999). Anti-cancer activity of targeted pro-apoptotic peptides. *Nat Med* **5**: 1032-1038.

36. Mai, JC, Mi, Z, Kim, SH, Ng, B, and Robbins, PD (2001). A proapoptotic peptide for the treatment of solid tumors. *Cancer Res* **61**: 7709-7712.

37. Marks, AJ, Cooper, MS, Anderson, RJ, Orchard, KH, Hale, G, North, JM, *et al.* (2005). Selective apoptotic killing of malignant hemopoietic cells by antibody-targeted delivery of an amphipathic peptide. *Cancer Res* **65**: 2373-2377.

38. Law, B, Quinti, L, Choi, Y, Weissleder, R, and Tung, CH (2006). A mitochondrial targeted fusion peptide exhibits remarkable cytotoxicity. *Mol Cancer Ther* **5**: 1944-1949.

39. Smolarczyk, R, Cichon, T, Graja, K, Hucz, J, Sochanik, A, and Szala, S (2006). Antitumor effect of RGD-4C-GG-D(KLAKLAK)2 peptide in mouse B16(F10) melanoma model. *Acta Biochim Pol* **53**: 801-805.

40. Kwon, MK, Nam, JO, Park, RW, Lee, BH, Park, JY, Byun, YR, *et al.* (2008). Antitumor effect of a transducible fusogenic peptide releasing multiple proapoptotic peptides by caspase-3. *Mol Cancer Ther* **7**: 1514-1522.

41. Borgne-Sanchez, A, Dupont, S, Langonne, A, Baux, L, Lecoeur, H, Chauvier, D, *et al.* (2007). Targeted Vpr-derived peptides reach mitochondria to induce apoptosis of alphaVbeta3-expressing endothelial cells. *Cell Death Differ* **14**: 422-435.

42. Guillemin, Y, Lopez, J, Gimenez, D, Fuertes, G, Valero, JG, Blum, L, *et al.* (2010). Active fragments from pro- and antiapoptotic BCL-2 proteins have distinct membrane behavior reflecting their functional divergence. *PLoS One* **5**: e9066.

43. Valero, JG, Sancey, L, Kucharczak, J, Guillemin, Y, Gimenez, D, Prudent, J, *et al.* (2011). Bax-derived membrane-active peptides act as potent and direct inducers of apoptosis in cancer cells. *Journal of cell science* **124**: 556-564.

44. Martinez-Abundis, E, Correa, F, Pavon, N, and Zazueta, C (2009). Bax distribution into mitochondrial detergent-resistant microdomains is related to ceramide and cholesterol content in postischemic hearts. *FEBS J* **276**: 5579-5588.

45. Martinez, F, Eschegoyen, S, Briones, R, and Cuellar, A (1988). Cholesterol increase in mitochondria: a new method of cholesterol incorporation. *J Lipid Res* **29**: 1005-1011.

46. Sancey, L, Ardisson, V, Riou, LM, Ahmadi, M, Marti-Batlle, D, Boturyn, D, *et al.* (2007). In vivo imaging of tumour angiogenesis in mice with the alpha(v)beta (3) integrin-targeted tracer 99mTc-RAFT-RGD. *Eur J Nucl Med Mol Imaging* **34**: 2037-2047.

47. Martinez-Abundis, E, Correa, F, Rodriguez, E, Soria-Castro, E, Rodriguez-Zavala, JS, Pacheco-Alvarez, D, *et al.* (2011). A CRAC-like motif in BAX sequence: relationship with protein insertion and pore activity in liposomes. *Biochim Biophys Acta* **1808**: 1888-1895.

48. Sohma, Y, and Kiso, Y (2006). "Click peptides"--chemical biology-oriented synthesis of Alzheimer's disease-related amyloid beta peptide (abeta) analogues based on the "O-acyl isopeptide method". *Chembiochem* **7**: 1549-1557.

49. Tuchscherer, G, Chandravarkar, A, Camus, MS, Berard, J, Murat, K, Schmid, A, *et al.* (2007). Switch-peptides as folding precursors in self-assembling peptides and amyloid fibrillogenesis. *Biopolymers* **88**: 239-252.

50. Foillard, S, Rasmussen, MO, Razkin, J, Boturyn, D, and Dumy, P (2008). 1-Ethoxyethylidene, a new group for the stepwise SPPS of aminooxyacetic acid containing peptides. *J Org Chem* **73**: 983-991.

51. Kim, JY, Han, JH, Park, G, Seo, YW, Yun, CW, Lee, BC, *et al.* (2016). Necrosis-inducing peptide has the beneficial effect on killing tumor cells through neuropilin (NRP-1) targeting. *Oncotarget*.

52. Qifan, W, Fen, N, Ying, X, Xinwei, F, Jun, D, and Ge, Z (2016). iRGD-targeted delivery of a pro-apoptotic peptide activated by cathepsin B inhibits tumor growth and metastasis in mice. *Tumour Biol*.

53. Jiang, L, Li, L, He, X, Yi, Q, He, B, Cao, J, *et al.* (2015). Overcoming drug-resistant lung cancer by paclitaxel loaded dual-functional liposomes with mitochondria targeting and pH-response. *Biomaterials* **52**: 126-139.

54. Chen, WH, Lei, Q, Yang, CX, Jia, HZ, Luo, GF, Wang, XY, *et al.* (2015). Bioinspired Nano-Prodrug with Enhanced Tumor Targeting and Increased Therapeutic Efficiency. *Small* **11**: 5230-5242.

55. Papo, N, Braunstein, A, Eshhar, Z, and Shai, Y (2004). Suppression of human prostate tumor growth in mice by a cytolytic D-, L-amino Acid Peptide: membrane lysis, increased necrosis, and inhibition of prostate-specific antigen secretion. *Cancer Res* **64**: 5779-5786.

56. Papo, N, Seger, D, Makovitzki, A, Kalchenko, V, Eshhar, Z, Degani, H*, et al.* (2006). Inhibition of tumor growth and elimination of multiple metastases in human prostate and breast xenografts by systemic inoculation of a host defense-like lytic peptide. *Cancer Res* **66**: 5371-5378.

57. Chen, Y, Xu, X, Hong, S, Chen, J, Liu, N, Underhill, CB*, et al.* (2001). RGD-Tachyplesin inhibits tumor growth. *Cancer Res* **61**: 2434-2438.

58. Bouchet, S, Tang, R, Fava, F, Legrand, O, and Bauvois, B (2015). The CNGRC-GG-D(KLAKLAK)2 peptide induces a caspase-independent, Ca2+-dependent death in human leukemic myeloid cells by targeting surface aminopeptidase N/CD13. *Oncotarget*.

59. Aouacheria, A, Combet, C, Tompa, P, and Hardwick, JM (2015). Redefining the BH3 Death Domain as a 'Short Linear Motif'. *Trends Biochem Sci* **40**: 736-748.

60. Vogler, M (2014). Targeting BCL2-Proteins for the Treatment of Solid Tumours. *Adv Med* **2014**: 943648.

61. Kolluri, SK, Zhu, X, Zhou, X, Lin, B, Chen, Y, Sun, K*, et al.* (2008). A short Nur77-derived peptide converts Bcl-2 from a protector to a killer. *Cancer Cell* **14**: 285-298.

62. Suzuki, M, Youle, RJ, and Tjandra, N (2000). Structure of Bax: coregulation of dimer formation and intracellular localization. *Cell* **103**: 645-654.

63. Annis, MG, Soucie, EL, Dlugosz, PJ, Cruz-Aguado, JA, Penn, LZ, Leber, B*, et al.* (2005). Bax forms multispanning monomers that oligomerize to permeabilize membranes during apoptosis. *Embo J* **24**: 2096-2103.

64. Cartron, PF, Arokium, H, Oliver, L, Meflah, K, Manon, S, and Vallette, FM (2005). Distinct domains control the addressing and the insertion of Bax into mitochondria. *J Biol Chem* **280**: 10587-10598.

65. Heimlich, G, McKinnon, AD, Bernardo, K, Brdiczka, D, Reed, JC, Kain, R*, et al.* (2004). Bax-induced cytochrome c release from mitochondria depends on alpha-helices-5 and -6. *Biochem J* **378**: 247-255.

66. Garcia-Saez, AJ, Chiantia, S, Salgado, J, and Schwille, P (2007). Pore formation by a Bax-derived peptide: effect on the line tension of the membrane probed by AFM. *Biophys J* **93**: 103-112.

67. Garcia-Saez, AJ, Coraiola, M, Dalla Serra, M, Mingarro, I, Menestrina, G, and Salgado, J (2005). Peptides derived from apoptotic Bax and Bid reproduce the poration activity of the parent full-length proteins. *Biophys J* **88**: 3976-3990.

68. Garcia-Saez, AJ, Coraiola, M, Serra, MD, Mingarro, I, Muller, P, and Salgado, J (2006). Peptides corresponding to helices 5 and 6 of Bax can independently form large lipid pores. *Febs J* **273**: 971-981.

69. Garcia-Saez, AJ, Mingarro, I, Perez-Paya, E, and Salgado, J (2004). Membrane-insertion fragments of Bcl-xL, Bax, and Bid. *Biochemistry* **43**: 10930-10943.

70. Qian, S, Wang, W, Yang, L, and Huang, HW (2008). Structure of transmembrane pore induced by Bax-derived peptide: evidence for lipidic pores. *Proc Natl Acad Sci U S A* **105**: 17379-17383.

71. Razkin, J, Josserand, V, Boturyn, D, Jin, ZH, Dumy, P, Favrot, M*, et al.* (2006). Activatable fluorescent probes for tumour-targeting imaging in live mice. *ChemMedChem* **1**: 1069-1072.

72. Green, DR, Ferguson, T, Zitvogel, L, and Kroemer, G (2009). Immunogenic and tolerogenic cell death. *Nat Rev Immunol* **9**: 353-363.

73. Zitvogel, L, Apetoh, L, Ghiringhelli, F, and Kroemer, G (2008). Immunological aspects of cancer chemotherapy. *Nat Rev Immunol* **8**: 59-73.

74. Aspord, C, Leccia, MT, Charles, J, and Plumas, J (2013). Plasmacytoid dendritic cells support melanoma progression by promoting Th2 and regulatory immunity through OX40L and ICOSL. *Cancer Immunol Res* **1**: 402-415.

Legends

Figure 1.
(A) Mitochondrial cytochrome c release assays with truncated Bax[106-134] peptide variants. Peptides at different concentrations (2.5 or 10μM) were incubated with isolated mitochondria for the indicated durations (min), and the presence of either mitochondrial-HSP70 or *Mitochondrial* Pyruvate dehydrogenase kinase 1 (mPDK1) and cytochrome c in the mitochondria (M) or in the mitochondrial supernatant (SN) were assessed by immunoblotting (IB). MOCK: control lanes with buffer-treated mitochondria. Mitochondria were purified from A375 cells. Among the assayed peptides (synthesized with L-amino acids), the first-generation peptide Bax[106-134] was active at 10μM, 6 peptides were inactive (italics), 2 were active at 10μM and Bax[109-127] was active at 2.5 μM (bold). Two truncated versions of this latter peptide lacking one or two C-terminal amino acids were inactive at 2.5μM (bottom). Bax[109-127] was selected as the minimal active peptide.
.

(B) (B) Mitochondrial cytochrome c release assays with the Bax[109-127] minimal active peptide using mitochondria isolated from various cancerous cell lines.
Mitochondria isolated from a variety of hematological (top panel) and melanoma (bottom) cell lines were incubated with the Bax[109-127] peptide at different concentrations for the indicated durations (min), and the presence of mPDK1 or cytochrome c in the mitochondria (M) or in the mitochondrial supernatant (SN) was assessed by immunoblotting (IB). MOCK: control lanes with buffer-treated mitochondria. For all the assayed cell lines except MeWo, mitochondrial cyt-c release was observed at 5μM after 5 min incubation with the peptide
(C) Mitochondrial cytochrome c release assays with the Bax[109-127] peptide in the all-D configuration.
Synthetic all-D peptides were incubated at the concentration of 10μM with isolated mitochondria for the indicated durations (min), and the presence of mPDK1 or cytochrome c in the mitochondria (M) or in the mitochondrial supernatant (SN) was assessed by immunoblotting (IB). MOCK: control lanes with buffer-treated mitochondria. Mitochondria were purified from Colo829 cells. A CGG triplet peptide was added to the N-terminal position of the Bax[109-127] peptide for allowing subsequent conjugation to the RAFT(cRGD) cargo. CGG-Bac[109-127]$_D$ induced cytochrome-c release in 5 min at a concentration of 10μM, whereas an N-terminally truncated variant peptide (Bax[115-127]$_D$) or a control peptide (CGG-Scr-Bax[109-127]$_D$) with a scrambled amino acid sequence of peptide Bax[109-127] were inactive (even at 25μM, not shown).

Figure 2: Synthesis of soluble depsi derivative of cgg-Poro2D

Figure 3: Synthesis of Poro-Combo compounds

Figure 4. Disulfide bridge formation of RAFT-(c[RGDfK-]$_4$) and depsi cgg-Poro2D peptide. HPLC traces of (a) RAFT-(c[RGDfK-]$_4$), (b) depsi cgg-Poro2D peptide, (c) RAFT-(c[RGDfK-]$_4$- depsi-cgg-Poro2D)

Figure 5: Evaluation of the impact of Poro-Combo (RAFT-c[RGD]$_4$-S-S-depsi-cgg-Poro2D) on cellular viability with a MTT test (A) on two melanoma cell lines Me275 (i) and Colo829 (ii). (B) Evaluation of the impact of Poro-Combo on cellular apoptosis by measuring Caspase
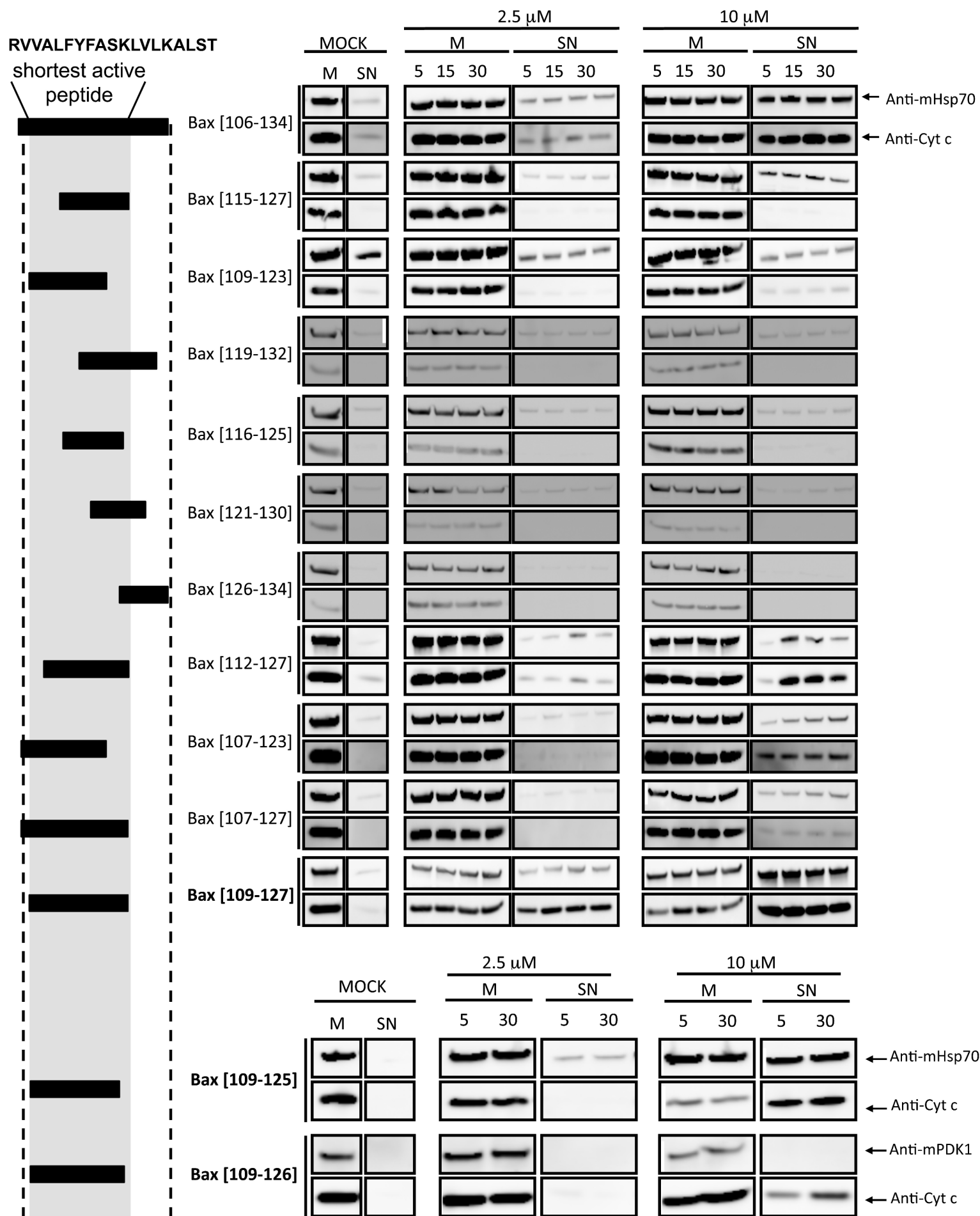
3 activation in three melanoma cell lines Me275 (i), Colo875 (ii) and A375 (iii). The control group received saline which is the vehicle for the other groups. Staurosporine (STS) is a positive control known to have a submicromolar IC50. Results are presented as mean ±SD. Statistical analysis were performed with Student t-test using GraphPad Prism$^®$ 6 software.

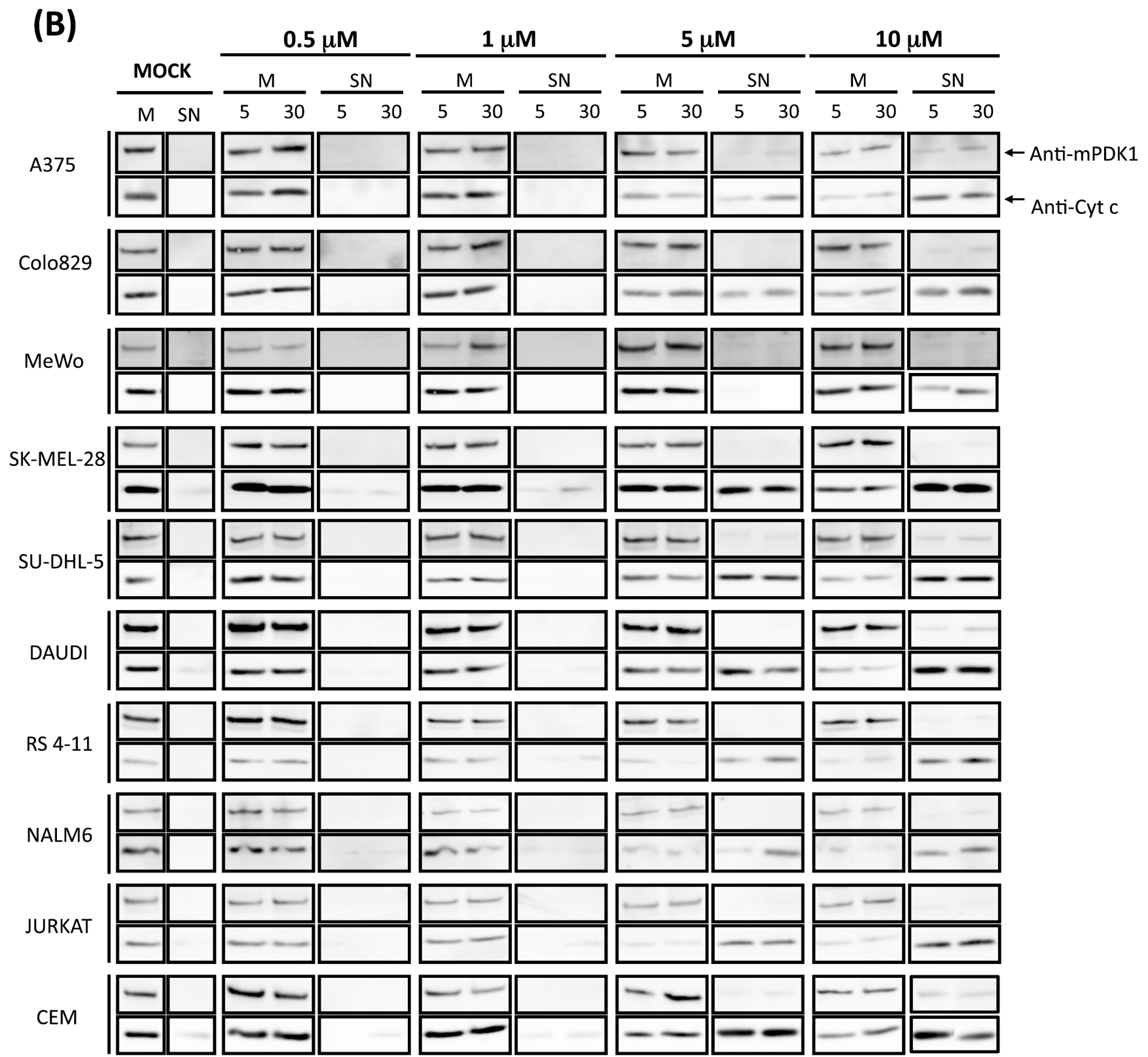**Figure 6**: Inhibition of *in vivo* tumor growth by RAFT-c(RGD)$_4$-poro2. (A) Melanoma cells Me275 were subcutaneously implanted on humice's right flank. After 6 days, mice received one daily intraperitoneal injection of saline (n=6), RAFT-c(RGD)$_4$ (n=8), poro2 (n=7), RAFT-c(RAD)$_4$-poro2 (n=4) or the treatment RAFT-c(RGD)$_4$-poro2 (n=7). Mice received injections between day 7 and day 13 (arrow). 24 hours after the last injection mice were sacrificed. Tumor volume was measured before and during the treatment. (B) At the end of the treatment, day 14, tumor volumes were compared between different groups of humice. Results are expressed as mean ± SEM. Statistical analysis were performed with Student t-test using GraphPad Prism® 6 software.

Figure 7: Poro-Combo induced cell proliferation inhibition and apoptosis *in vivo*. Representative images of sections from tumor xenografts obtained from control mice or mice treated with RAFT-cRGD, Poro2, RAFT-RAD-poro2 or Poro-Combo peptides, as indicated. Staining of Ki-67, a proliferation marker (left column, objective x40), active caspase-3 to measure apoptosis (middle column, objective x40), and of CD31 to visualize angiogenesis (right column, objective x10) were shown. Tumor slides from control and treated mice were visualized under microscope and Ki67 and cleaved caspase-3 positive cells were quantified. Six fields per sample were analyzed, counting 1000 cells per slide in randomly selected fields. Histograms represent the percentage of Ki67 and cleaved caspase-3 positive cells ± SEM in 4 mice. CD31 staining was counted in ten randomly selected fields. Data represent the arithmetic mean of CD31 per field ± SEM of 4 mice.
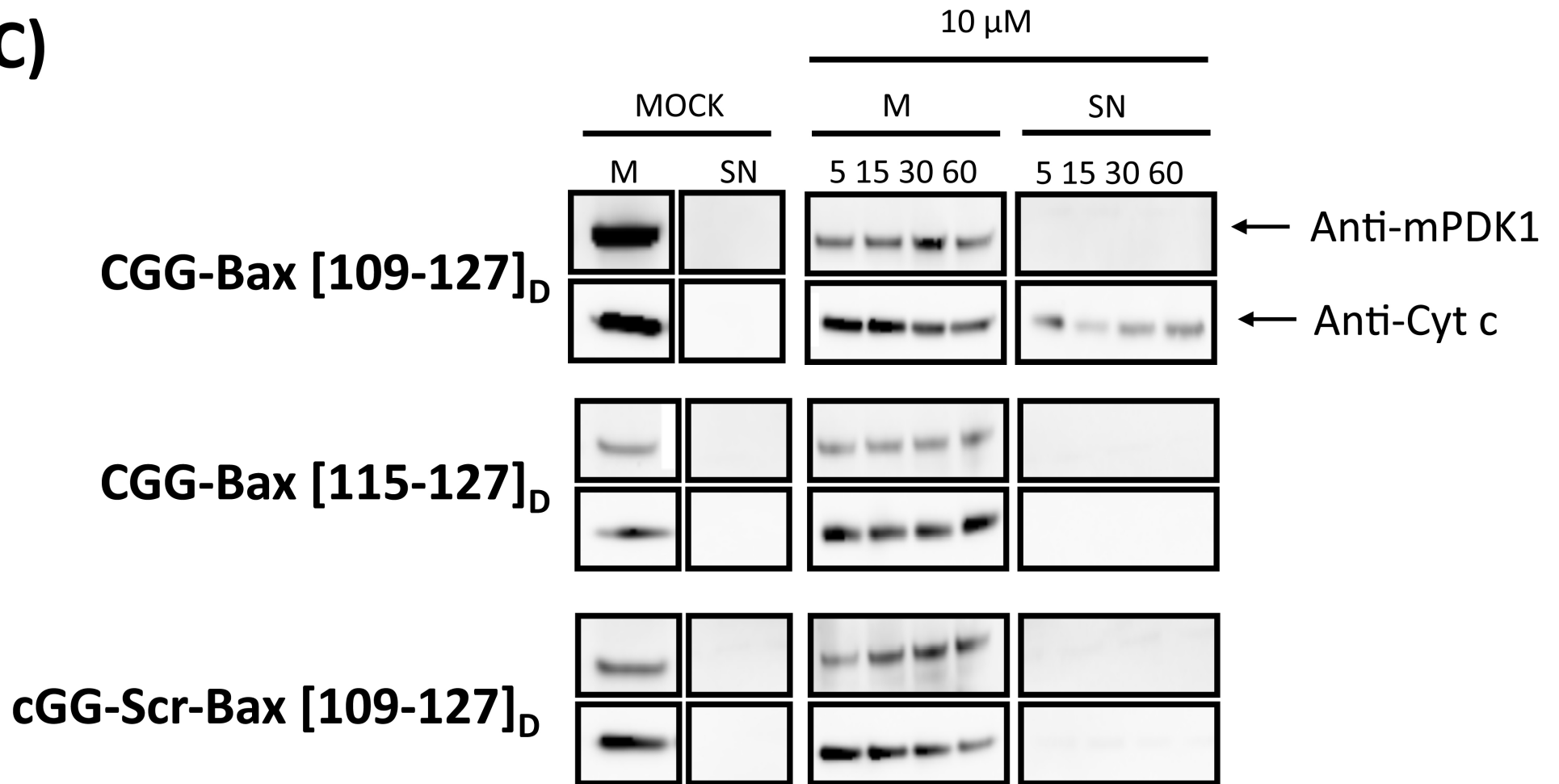
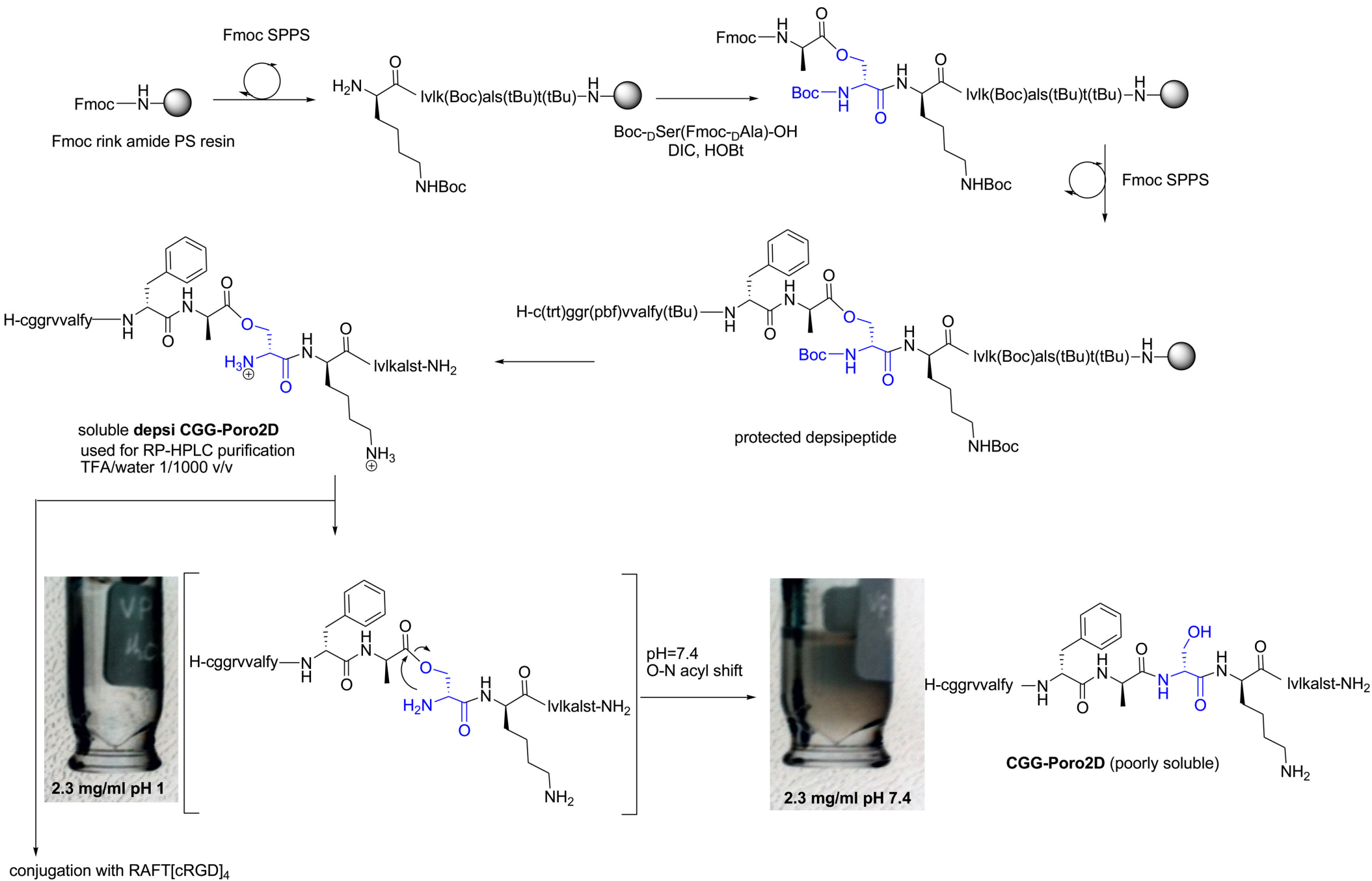**Figure 8 : Impact of RAFT-c(RGD)4-poro2 treatment on angiogenic factors and chemokines in the plasma**
Melanoma cells Me275 were subcutaneously implanted on Humice's right flank. After 6 days, mice received one daily intraperitoneal injection of saline (n=6), RAFT-c(RGD)4 (n=8), poro2 (n=7), RAFT-c(RAD)4-poro2 (n=4) or RAFT-c(RGD)4-poro2 (n=6). Angiogenic factors and immune-related chemokines were quantified in the plasma of mice at different time points. (A) Quantification of human angiogenin and FGF-2. (B) Quantification of human MCP1 and IP10.
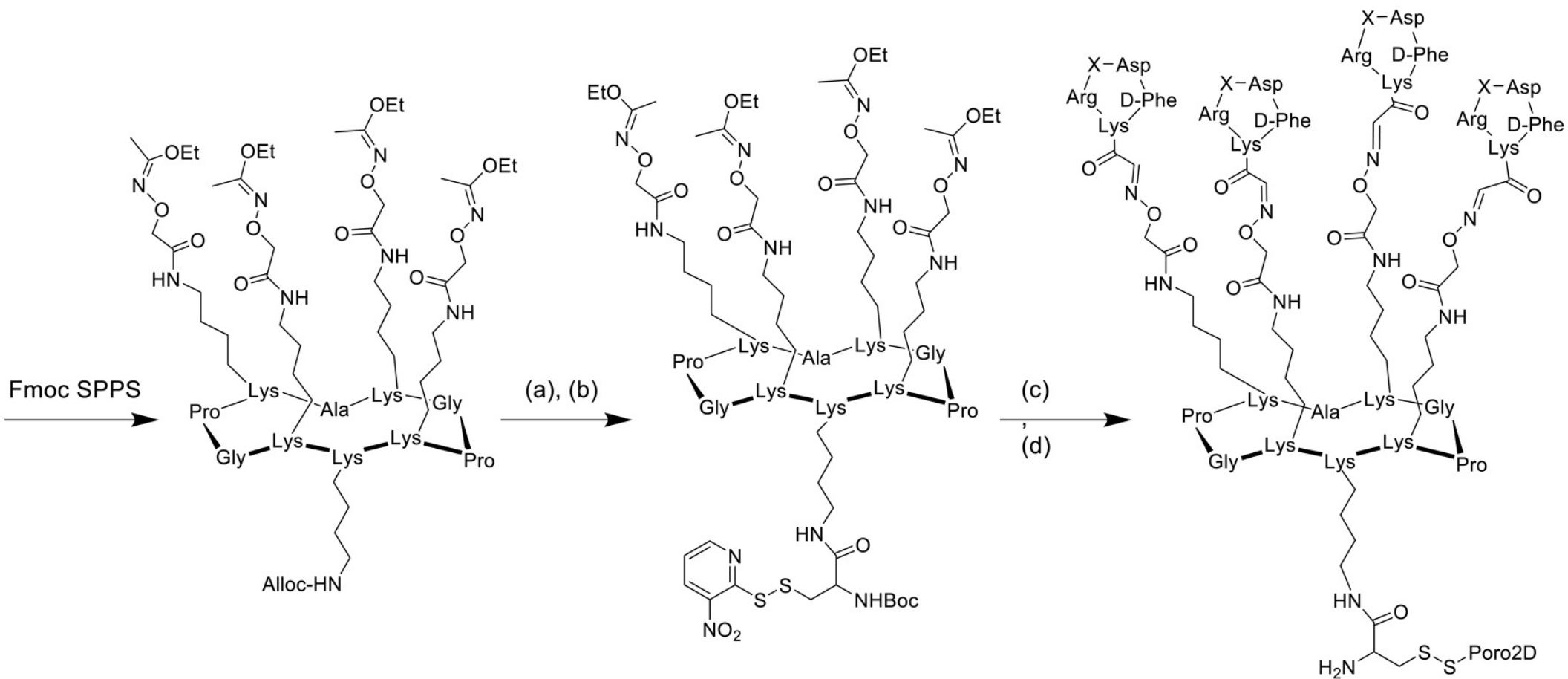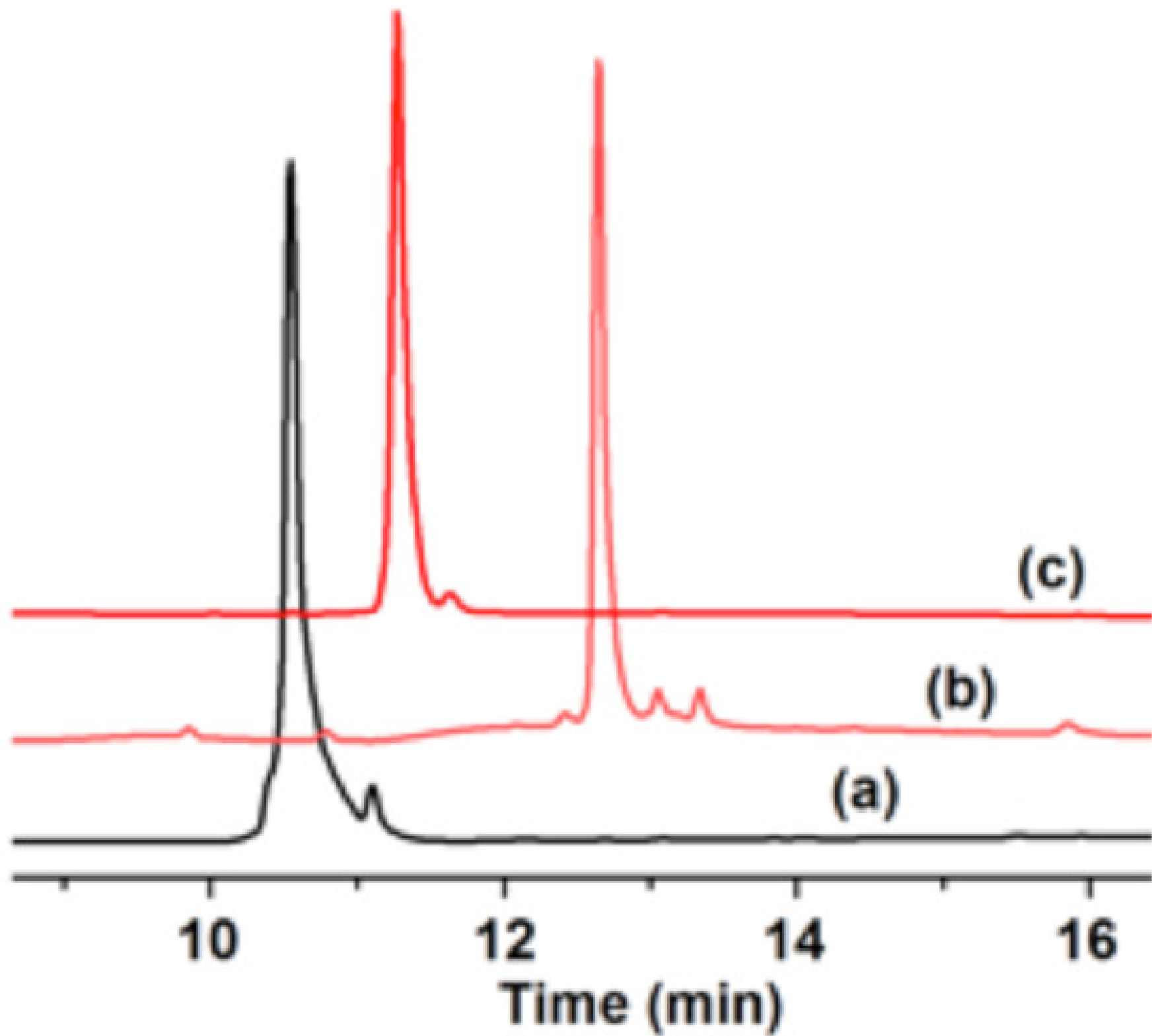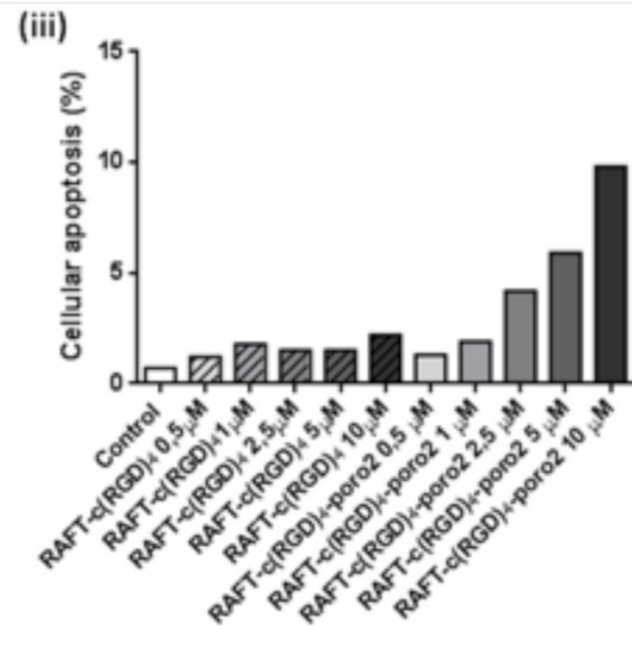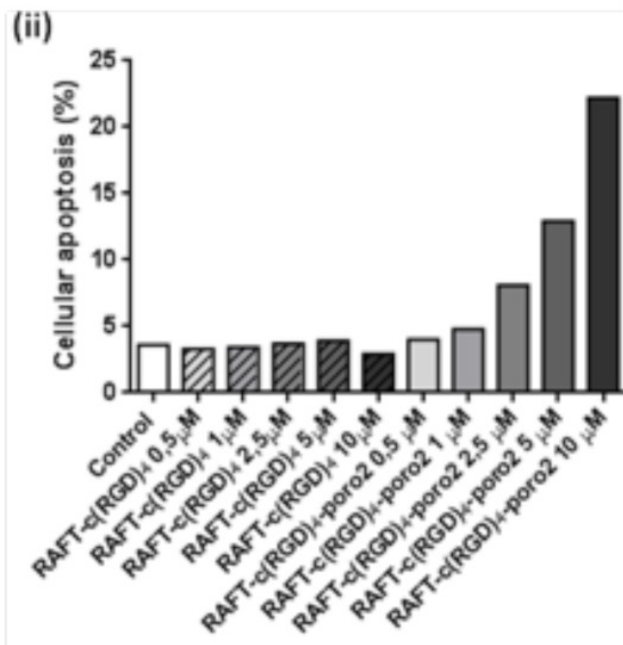
(A)

RVVALFYFASKLVLKALST
shortest active peptide

	MOCK		2.5 μM		10 μM	
	M	SN	M	SN	M	SN
			5 15 30	5 15 30	5 15 30	5 15 30

Bax [106-134] ← Anti-mHsp70
← Anti-Cyt c

Bax [115-127]

Bax [109-123]

Bax [119-132]

Bax [116-125]

Bax [121-130]

Bax [126-134]

Bax [112-127]

Bax [107-123]

Bax [107-127]

Bax [109-127]

	MOCK		2.5 μM		10 μM	
	M	SN	M	SN	M	SN
			5 30	5 30	5 30	5 30

Bax [109-125] ← Anti-mHsp70
← Anti-Cyt c

Bax [109-126] ← Anti-mPDK1
← Anti-Cyt c

(B)

(C)

Fmoc SPPS

Fmoc rink amide PS resin

Boc-DSer(Fmoc-DAla)-OH
DIC, HOBt

Fmoc SPPS

H-c(trt)ggr(pbf)vvalfy(tBu)

soluble **depsi CGG-Poro2D**
used for RP-HPLC purification
TFA/water 1/1000 v/v

protected depsipeptide

2.3 mg/ml pH 1

pH=7.4
O-N acyl shift

2.3 mg/ml pH 7.4

CGG-Poro2D (poorly soluble)

conjugation with RAFT[cRGD]$_4$

Fmoc SPPS →

(a), (b) →

(c), (d) →

X = Gly : RAFT-(c[-RGDfK-])$_4$-Poro2D

X = βAla : RAFT-(c[-RβADfK-])$_4$-Poro2D

(c)

(b)

(a)

A. (i) Cellular viability (%) — Control, STS 1 μM, RAFT-c(RGD)₄-poro2 1 μM, RAFT-c(RGD)₄-poro2 2.5 μM, RAFT-c(RGD)₄-poro2 5 μM, RAFT-c(RGD)₄-poro2 10 μM

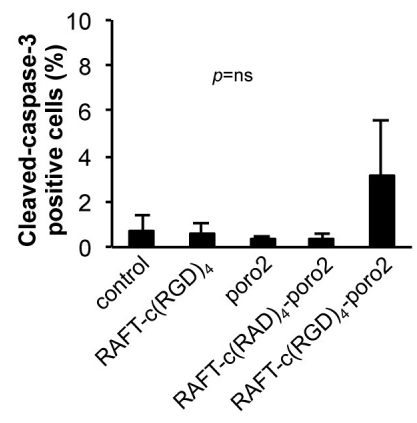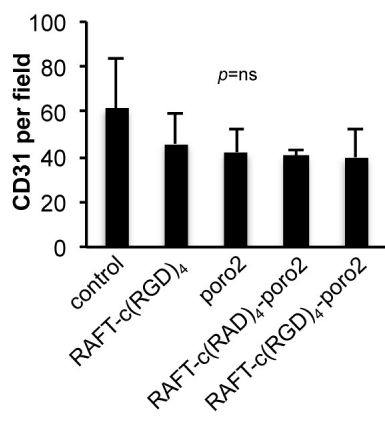(ii) Cellular viability (%) — control, STS 1 μM, RAFT-c(RGD)₄-poro2 1 μM, RAFT-c(RGD)₄-poro2 2.5 μM, RAFT-c(RGD)₄-poro2 5 μM, RAFT-c(RGD)₄-poro2 10 μM

B. (i) Cellular apoptosis (%) — control, RAFT-c(RGD)₄ 0.5 μM, RAFT-c(RGD)₄ 1 μM, RAFT-c(RGD)₄ 2.5 μM, RAFT-c(RGD)₄ 5 μM, RAFT-c(RGD)₄ 10 μM, RAFT-c(RGD)₄-poro2 0.5 μM, RAFT-c(RGD)₄-poro2 1 μM, RAFT-c(RGD)₄-poro2 2.5 μM, RAFT-c(RGD)₄-poro2 5 μM, RAFT-c(RGD)₄-poro2 10 μM

(ii) Cellular apoptosis (%)

(iii) Cellular apoptosis (%)

	Ki67 (x40)	Active caspase-3 (x40)	CD31 (x10)

Columns (left to right): **Ki67** (x40), **Active caspase-3** (x40), **CD31** (x10)

Rows (top to bottom): control, RAFT-c(RGD)$_4$, Poro2, RAFT-c(RAD)$_4$-poro2, RAFT-c(RGD)$_4$-poro2

Bottom graphs:

Ki67 positive cells (%) — * p=0.0105
X-axis: control, RAFT-c(RGD)$_4$, poro2, RAFT-c(RAD)$_4$-poro2, RAFT-c(RGD)$_4$-poro2

CD31 per field — p=ns
X-axis: control, RAFT-c(RGD)$_4$, poro2, RAFT-c(RAD)$_4$-poro2, RAFT-c(RGD)$_4$-poro2

Cleaved-caspase-3 positive cells (%) — p=ns
X-axis: control, RAFT-c(RGD)$_4$, poro2, RAFT-c(RAD)$_4$-poro2, RAFT-c(RGD)$_4$-poro2